UNIVERSITY OF AMSTERDAM

UvA-DARE (Digital Academic Repository)

Probing the Maximum Energy of Fast Radio Bursts Using Thousands of Sources from the Second CHIME/FRB Catalog

Shah, Vishwangi; Hessels, Jason W.T.; Kaspi, Victoria M.; Masui, Kiyoshi W.; Sammons, Mawson W.; Amouyal, Daniel; Brar, Charanjot; Chatterjee, Shami; Curtin, Alice P.; Didehbani, Hannah; Gaensler, B.M.; Jain, Naman; Joseph, Ronniy C.; Khan, Afrokk; Kharel, Bikash; Lanman, Adam E.; McGregor, Kyle; Mckinven, Ryan; Ng, Mason; Nimmo, Kenzie; Pandhi, Ayush; Pearlman, Aaron B.; Pollak, Alexander W.; Scholz, Paul; Shin, Kaitlyn; Siegel, Seth R.; Smith, Kendrick; Woodland, Michele

DOI
10.3847/1538-4357/ae9a96

Publication date
2026

Document Version
Final published version

Published in
Astrophysical Journal

License
CC BY

Link to publication

Citation for published version (APA):
Shah, V., Hessels, J. W. T., Kaspi, V. M., Masui, K. W., Sammons, M. W., Amouyal, D., Brar, C., Chatterjee, S., Curtin, A. P., Didehbani, H., Gaensler, B. M., Jain, N., Joseph, R. C., Khan, A., Kharel, B., Lanman, A. E., McGregor, K., Mckinven, R., Ng, M., ... Woodland, M. (2026). Probing the Maximum Energy of Fast Radio Bursts Using Thousands of Sources from the Second CHIME/FRB Catalog. *Astrophysical Journal*, *1009*(2), Article 155. https://doi.org/10.3847/1538-4357/ae9a96

General rights
It is not permitted to download or to forward/distribute the text or part of it without the consent of the author(s) and/or copyright holder(s), other than for strictly personal, individual use, unless the work is under an open content license (like Creative Commons).

UvA-DARE is a service provided by the library of the University of Amsterdam (https://dare.uva.nl)

Disclaimer/Complaints regulations
If you believe that digital publication of certain material infringes any of your rights or (privacy) interests, please let the Library know, stating your reasons. In case of a legitimate complaint, the Library will make the material inaccessible and/or remove it from the website. Please Ask the Library: https://uba.uva.nl/en/contact, or a letter to: Library of the University of Amsterdam, Secretariat, P.O. Box 19185, 1000 GD Amsterdam, The Netherlands. You will be contacted as soon as possible.

Download date:17 Nov 2026

The Astrophysical Journal, 1009:155 (12pp), 2026 October 1 https://doi.org/10.3847/1538-4357/ae9a96
© 2026. The Author(s). Published by the American Astronomical Society.
OPEN ACCESS

Probing the Maximum Energy of Fast Radio Bursts Using Thousands of Sources from the Second CHIME/FRB Catalog

Vishwangi Shah[1,2], Jason W. T. Hessels[1,2,3,4], Victoria M. Kaspi[1,2,5], Kiyoshi W. Masui[6,7], Mawson W. Sammons[1,2], Daniel Amouyal[1,2], Charanjot Brar[8], Shami Chatterjee[9], Alice P. Curtin[1,2], Hannah Didehbani[7], B. M. Gaensler[10,11,12], Naman Jain[1,2], Ronniy C. Joseph[1,2], Afrokk Khan[1,2], Bikash Kharel[13,14], Adam E. Lanman[6,7], Kyle McGregor[1,2], Ryan Mckinven[1,2], Mason Ng[1,2], Kenzie Nimmo[15], Ayush Pandhi[1,2], Aaron B. Pearlman[1,2,6,7,20], Alexander W. Pollak[16], Paul Scholz[17], Kaitlyn Shin[18], Seth R. Siegel[1,2,19], Kendrick Smith[19], and Michele Woodland[10]

[1] Department of Physics, McGill University, 3600 rue University, Montréal, QC H3A 2T8, Canada; vishwangi.shah@mail.mcgill.ca
[2] Trottier Space Institute, McGill University, 3550 rue University, Montréal, QC H3A 2A7, Canada
[3] Anton Pannekoek Institute for Astronomy, University of Amsterdam, Science Park 904, 1098 XH Amsterdam, The Netherlands
[4] ASTRON, Netherlands Institute for Radio Astronomy, Oude Hoogeveensedijk 4, 7991 PD Dwingeloo, The Netherlands
[5] School of Physics and Astronomy, Tel Aviv University, Tel Aviv 69978, Israel
[6] MIT Kavli Institute for Astrophysics and Space Research, Massachusetts Institute of Technology, 77 Massachusetts Ave, Cambridge, MA 02139, USA
[7] Department of Physics, Massachusetts Institute of Technology, 77 Massachusetts Avenue, Cambridge, MA 02139, USA
[8] NRC Herzberg Astronomy and Astrophysics, 5071 West Saanich Road, Victoria, BC V9E2E7, Canada
[9] Cornell Center for Astrophysics and Planetary Science, Cornell University, Ithaca, NY 14853, USA
[10] Department of Astronomy and Astrophysics, University of California Santa Cruz, 1156 High Street, Santa Cruz, CA 95064, USA
[11] David A. Dunlap Department of Astronomy and Astrophysics, 50 St. George Street, University of Toronto, ON M5S 3H4, Canada
[12] Dunlap Institute for Astronomy and Astrophysics, 50 St. George Street, University of Toronto, ON M5S 3H4, Canada
[13] Department of Physics and Astronomy, West Virginia University, PO Box 6315, Morgantown, WV 26506, USA
[14] Center for Gravitational Waves and Cosmology, West Virginia University, Chestnut Ridge Research Building, Morgantown, WV 26505, USA
[15] Center for Interdisciplinary Exploration and Research in Astronomy (CIERA), Northwestern University, 1800 Sherman Avenue, Evanston, IL 60201, USA
[16] SETI Institute, Mountain View, CA, USA
[17] Department of Physics and Astronomy, York University, 4700 Keele Street, Toronto, ON MJ3 1P3, Canada
[18] Cahill Center for Astronomy and Astrophysics, MC 249-17 California Institute of Technology, Pasadena CA 91125, USA
[19] Perimeter Institute of Theoretical Physics, 31 Caroline Street North, Waterloo, ON N2L 2Y5, Canada
Received 2026 February 22; revised 2026 August 5; accepted 2026 August 13; published 2026 September 25

Abstract

Quantifying the maximum energy of fast radio bursts (FRBs) can provide stringent constraints on their emission mechanisms and progenitor models. However, the most energetic bursts are rare, requiring a large sample of FRBs to detect them. In this work, we use the largest available such sample, 2998 one-off FRBs from the Second CHIME/FRB Catalog, to obtain a lower limit on the maximum energy ($E_{\rm iso}^{\rm max}$) of FRBs, assuming isotropic energy distribution from FRB sources. In the absence of known redshifts (z) for most sources, we present a framework that uses the dispersion measures (DMs) and fluences of these FRBs, together with the probability distribution of z given DM, to derive the lower limit on $E_{\rm iso}^{\rm max}$. We generate simulated FRB samples assuming different parameter values for a log-normal $\rm DM_{host}$ distribution and a Schechter function form of the FRB energy function to estimate how many outliers—FRBs with large DM contributions from the host galaxy or intervening galaxy halos—could artificially inflate this limit. After accounting for outliers, the lower limit on $E_{\rm iso}^{\rm max}$ from Catalog 2 FRBs ranges between 1.1×10^{41} and 1.9×10^{42} erg, with best estimate 1.5×10^{42} erg. This limit is consistent with estimates of the Schechter function cutoff energy ($E_{\rm iso}^{\rm cutoff}$) derived from much smaller FRB samples. Moreover, inferred energies of hundreds of FRBs appear collectively limited around $\sim 10^{42}$ erg, suggesting a physical limit on the energy reservoir of FRB sources. The corresponding isotropic-equivalent FRB source energy is consistent with the total energy available in a magnetar's external dipole magnetic field, supporting magnetars as FRB progenitors.

Unified Astronomy Thesaurus concepts: Radio bursts (1339); Radio transient sources (2008); Magnetars (992); High energy astrophysics (739)

1. Introduction

Fast radio bursts (FRBs) are extremely energetic radio transients, having isotropic equivalent energies ranging over 10^{37}–10^{42} erg, packed into millisecond time durations, making them detectable at cosmological distances of millions to billions of parsecs (E. Petroff et al. 2022). First detected in 2007 (D. R. Lorimer et al. 2007), thousands of FRBs have now been reported (CHIME/FRB Collaboration et al. 2026); however, their origins remain a mystery. About ∼3% of FRBs have been observed to repeat (CHIME/FRB Collaboration et al. 2021, 2023), ruling out cataclysmic origins for at least this class of FRBs. The clues for FRB progenitors and emission mechanisms can be found in their burst properties as well as the kind of galaxies and local environments in which they occur. Their millisecond duration points toward compact object progenitors, and microsecond-duration bursts and sub-bursts observed from some FRB sources (K. Nimmo et al. 2022;

[20] NASA Hubble Fellow.

Original content from this work may be used under the terms of the Creative Commons Attribution 4.0 licence. Any further distribution of this work must maintain attribution to the author(s) and the title of the work, journal citation and DOI.

M. P. Snelders et al. 2023), provide evidence that the bursts are generated in the magnetospheres of neutron stars. The varying polarization angle features in bursts from repeating FRBs (R. Luo et al. 2020b) and a neutron-star-like polarization position angle swing in at least one FRB source (R. Mckinven et al. 2024), further support magnetospheric origin of FRBs. Their high brightness temperatures ($T_B > 10^{32}$ K) imply a coherent emission process, whereby reconnection in the neutron-star magnetosphere (M. Lyutikov & S. Popov 2020; M. Lyutikov 2021), or magnetar flares colliding with the surrounding medium (Y. Lyubarsky 2014; B. D. Metzger et al. 2019), are the most favored FRB emission theories. The preferential occurrence of FRBs in star-forming galaxies supports magnetars formed via core-collapse supernovae of massive stars as progenitors (K. E. Heintz et al. 2020; S. Bhandari et al. 2022; A. C. Gordon et al. 2023; M. Bhardwaj et al. 2024; K. Sharma et al. 2024). However, some FRBs localized to quiescent environments suggest alternative formation channels for FRB progenitors (F. Kirsten et al. 2022; K. Sharma et al. 2024; T. Eftekhari et al. 2025; V. Shah et al. 2025).

The maximum isotropic energy ($E_{\rm iso}^{\rm max}$) of FRBs can provide an effective way to examine the viability of the various FRB emission mechanisms and progenitor models. FRBs could be beamed, but their beaming fraction is unknown, so isotropic emission is typically assumed when estimating energy. The most energetic FRBs yet detected, having $E_{\rm iso} \sim 10^{42}$ erg (V. Ravi et al. 2019; S. D. Ryder et al. 2023), are reaching the limits of what a magnetar could produce from external dipolar magnetic fields, given the standard assumptions for radio efficiencies ($\eta_{\rm radio} \lesssim 10^{-4}$; C. D. Bochenek et al. 2020) and surface dipolar field strength ($B_P = 10^{15}$ G). Bursts more energetic than this could imply extreme values for these parameters, energy released from stronger multipole components of the magnetar magnetic field, upper limits on the beaming fraction of FRBs, or a different progenitor altogether. However, the energy range of detected FRBs is limited by the sensitivity of radio telescopes on one end, and by the low rates of highly energetic bursts on the other end (C. W. James et al. 2022; K. Shin et al. 2023; F. Kirsten et al. 2024; O. S. Ould-Boukattine et al. 2024). The rare nature of the most energetic bursts necessitates a large sample of FRBs to be able to detect them. The Second CHIME/FRB Catalog (hereafter referred to as Catalog 2) comprises 4539 FRBs originating from 3641 unique sources (CHIME/FRB Collaboration et al. 2026), and provides an opportunity to probe unusually energetic FRBs.

To constrain the FRB energy distribution, previous works have performed population modeling of FRBs by fitting their observed fluence and DMs to models comprising the spectral index of FRBs (α) and assumed functions for the FRB energy distribution, star formation rate, and host-galaxy DM ($\rm DM_{host}$) distribution (R. Luo et al. 2020a; C. W. James et al. 2022; K. Shin et al. 2023). In most of these works, the FRB energy distribution is modeled as a Schechter function, which is a power law with index γ and an exponential energy cutoff at $E_{\rm iso}^{\rm cutoff}$ at the high-energy end. $\rm DM_{host}$ is modeled as a log-normal distribution with mean $\mu_{\rm host}$ and standard deviation $\sigma_{\rm host}$. These free parameters are simultaneously varied to obtain the best-fit values that explain the observed data, while taking into account selection biases of the telescope. Such a population modeling of Catalog 2 FRBs will be presented in an upcoming work (N. Jain et al. 2026, in preparation). Other works, such as W. R. Arcus et al. (2025), have used the model-independent $V/V_{\rm max}$ method, which can determine the energy distribution of FRBs without assuming a functional form of the FRB energy function but requires accurate determination of the FRB location within the telescope beam. Such a method cannot be applied to Catalog 2 FRBs, most of which have a wide localization region and poorly constrained locations within the CHIME/FRB telescope beam.

In the Schechter function formalism, the highest-energy FRBs beyond $E_{\rm iso}^{\rm cutoff}$ are not directly probed. Moreover, the energy distribution of FRBs might not necessarily be a Schechter function. In this work, we use a framework independent of the assumed form of the FRB energy function to probe the highest-energy FRBs in the Catalog 2 sample and constrain the maximum energy of FRBs.

The dataset used in this work is discussed in Section 2; the methods used to estimate and verify our results are described in Section 3. The lower limit on $E_{\rm iso}^{\rm max}$ value that we derive is presented in Section 4, and the resulting implications for the progenitors of FRBs are discussed in Section 5.

2. Dataset

The Canadian Hydrogen Intensity Mapping Experiment (CHIME) is a transit radio telescope located in Penticton, British Columbia and operates in the 400–800 MHz frequency band (CHIME Collaboration 2022). It consists of four 100×20 m cylindrical paraboloidal reflectors that provide a $\gtrsim 200$ deg^2 instantaneous field of view (FOV). CHIME's FRB search engine makes use of this large FOV, its powerful correlator, and wide bandwidth to search the entire Northern sky every day for FRBs (CHIME/FRB Collaboration 2018). This makes CHIME/FRB the leader in FRB discovery rate, observing $\sim$3 FRBs per day.

Catalog 2 (CHIME/FRB Collaboration et al. 2026) reports on 4539 bursts, including 981 bursts from 83 known repeating sources, detected by CHIME/FRB between 2018 July and 2023 September. It also characterizes the properties of these bursts, including DMs, temporal widths, scattering times, fluences, etc., and presents a $O(10')$ sky localization for each source. The large localization uncertainty prevents host galaxy association and, thus, redshift (z) determination for most of these FRBs. The reported fluences are lower limits, as in the absence of accurate sky location, the bursts are assumed to be detected at the location of the primary beam's highest sensitivity in the FRB's declination arc on the sky (B. C. Andersen et al. 2023).

In this work, we use the DMs and fluence lower limits of one-off FRBs presented in Catalog 2. We decided to exclude repeating FRBs because they are known to often have distinct burst morphologies compared to apparently one-off FRBs (Z. Pleunis et al. 2021; A. P. Curtin et al. 2025), possibly resulting in different detection biases between the two subsamples. Our sample also excludes FRBs that have extragalactic DMs less than 100 pc cm^{-3} and FRBs that do not have reported fluence measurements due to calibration issues or RFI contamination. Additionally, as suggested in CHIME/FRB Collaboration et al. (2026), we remove FRBs detected during periods of nonnominal system sensitivity and those discovered by citizen scientists. We also remove far side-lobe events, which can be orders of magnitude brighter than main lobe events but have poorly understood beam response and, thus, do not have reported fluence values in CHIME/FRB Collaboration et al. (2026). This leaves 2998 unique FRB sources having the required DM and fluence information, which we then combine with the probability distribution

function (PDF) of z given DM, $P(z|\mathrm{DM})$, to estimate a lower limit on $E_{\mathrm{iso}}^{\mathrm{max}}$, as described in Section 3.

3. Methods

In Section 3.1, we present our framework for obtaining a lower limit on $E_{\mathrm{iso}}^{\mathrm{max}}$ using the DMs and fluences of a sample of FRBs. To test the performance of this method, we apply it to simulated FRB samples and compare the obtained lower limit on $E_{\mathrm{iso}}^{\mathrm{max}}$ to the true $E_{\mathrm{iso}}^{\mathrm{max}}$ in the sample. The simulated samples are generated using the steps and assumptions described in Section 3.2. In Section 3.3, we develop a method to use the simulated samples to estimate the number of outlier FRBs that can falsely inflate the lower limit on $E_{\mathrm{iso}}^{\mathrm{max}}$ due to excess DM from the host or intervening halos. We obtain the lower limit on $E_{\mathrm{iso}}^{\mathrm{max}}$ from Catalog 2 FRBs after accounting for the outliers.

3.1. Framework to Obtain Lower Limit on $E_{\mathrm{iso}}^{\mathrm{max}}$

The observed DM of an FRB can be expressed as the sum of various components,

$$\mathrm{DM}(z) = \mathrm{DM}_{\mathrm{MW,ISM}} + \mathrm{DM}_{\mathrm{MW,halo}} + \mathrm{DM}_{\mathrm{cosmic}}(z) + \frac{\mathrm{DM}_{\mathrm{host}}}{1+z}. \tag{1}$$

$\mathrm{DM}_{\mathrm{MW,ISM}}$ and $\mathrm{DM}_{\mathrm{MW,halo}}$ are the contributions from the interstellar medium (ISM) and halo of the Milky Way (MW), respectively. $\mathrm{DM}_{\mathrm{cosmic}}$ is from the ionized gas in the intergalactic medium (IGM) and any intervening galaxy halos along the line of sight. It depends on the path length through the IGM and, thus, is a function of redshift (z). $\mathrm{DM}_{\mathrm{host}}$ is the DM contributed by the host galaxy of the FRB, which is converted to the observer's frame by the $1+z$ factor.

To calculate the energies of FRBs, their redshifts are required. In the absence of known redshifts, we can use the dependence of DM on z to obtain $P(z|\mathrm{DM})$, and translate that to a PDF of E_{iso} given DM, $P(E_{\mathrm{iso}}|\mathrm{DM})$, using the following steps:

1. Using the Bayes' theorem:

$$P(z|\mathrm{DM}) \propto P(\mathrm{DM}|z) \times P(z). \tag{2}$$

   For a grid of z ranging between 0.01 and 6, we assume a flat, uninformative prior for $P(z)$. $P(z|\mathrm{DM})$ is certainly dependent on the selection biases of the telescope, such as the $P(z|\mathrm{DM})$ presented in K. Shin et al. (2023) for FRBs detected by CHIME/FRB. However, here we choose to construct a telescope-independent $P(z|\mathrm{DM})$. We develop a method to account for selection effects post facto in Sections 3.2, 3.3, and 4.
2. For $P(\mathrm{DM}|z)$, we marginalize over $\mathrm{DM}_{\mathrm{host}}$ and $\mathrm{DM}_{\mathrm{MW}}$ to obtain

$$P(\mathrm{DM}|z) \propto \int\int d\mathrm{DM}_{\mathrm{MW}}\, d\mathrm{DM}_{\mathrm{host}} \times P(\mathrm{DM}_{\mathrm{MW}})\, P\left(\mathrm{DM}_{\mathrm{cosmic}} = \mathrm{DM} - \mathrm{DM}_{\mathrm{MW}} - \frac{\mathrm{DM}_{\mathrm{host}}}{1+z}|z\right) P(\mathrm{DM}_{\mathrm{host}}), \tag{3}$$

   where $\mathrm{DM}_{\mathrm{MW}}$ is the sum of $\mathrm{DM}_{\mathrm{MW,ISM}}$ and $\mathrm{DM}_{\mathrm{MW,halo}}$. We present a more detailed derivation of this form of $P(\mathrm{DM}|z)$ in Appendix A.
3. We use a parameterization of $P(\mathrm{DM}_{\mathrm{cosmic}}|z)$ (M. McQuinn 2014; J. P. Macquart et al. 2020) that takes into account filaments and intervening halos to give a probabilistic distribution of ionized gas in the Universe about a mean value:

$$P(\mathrm{DM}_{\mathrm{cosmic}}|z) = \langle \mathrm{DM}_{\mathrm{cosmic}} \rangle P(\Delta_{\mathrm{DM}}). \tag{4}$$

   $\langle \mathrm{DM}_{\mathrm{cosmic}} \rangle$ is the mean cosmological DM as a function of z, which, assuming a flat Universe with matter and dark energy, can be written as

$$\langle \mathrm{DM}_{\mathrm{cosmic}} \rangle (z) = \int_0^z \frac{c\, \bar{n}_e(z')\, dz'}{H_0(1+z')^2 \sqrt{\Omega_m(1+z')^3 + \Omega_\Lambda}}, \tag{5}$$

   where $\bar{n}_e(z')$ is the mean density of free electrons, and we assume Planck cosmology with $H_0 = 67.4\,\mathrm{km\,s^{-1}}$, matter density $\Omega_m = 0.315$, and dark energy density $\Omega_\Lambda = 0.685$ (Planck Collaboration et al. 2020). Δ_{DM} is the deviation from the mean caused by intersections with galactic halos along the line of sight, such that $P(\Delta_{\mathrm{DM}})$ can be written as:

$$P(\Delta_{\mathrm{DM}})(z) = A\Delta_{\mathrm{DM}}^{-\beta} \exp\left[-\frac{(\Delta_{\mathrm{DM}}^{-\alpha} - C_0)^2}{2\alpha^2 \sigma_{\mathrm{DM}}(z)^2}\right], \tag{6}$$

   where we use the model parameter values from C. W. James et al. (2022). $\sigma_{\mathrm{DM}}(z) = Fz^{-0.5}$, where the feedback parameter F quantifies the strength with which galaxies expel baryons. Our implementation of $P(\mathrm{DM}_{\mathrm{cosmic}}|z)$ is based on the `grid_P_DMcosmic_z` function in the public `FRB`[21] GitHub repository.
4. We assume $\mathrm{DM}_{\mathrm{host}}$ values between 1 and 1000 $\mathrm{pc\,cm^{-3}}$ with $P(\mathrm{DM}_{\mathrm{host}})$ given by a log-normal distribution of the form

$$P(\mathrm{DM}_{\mathrm{host}}) = \frac{1}{\mathrm{DM}_{\mathrm{host}}} \frac{1}{\sigma_{\mathrm{host}}\sqrt{2\pi}} e^{-\frac{(\log \mathrm{DM}_{\mathrm{host}} - \mu_{\mathrm{host}})^2}{2\sigma_{\mathrm{host}}^2}}, \tag{7}$$

   where $\mu_{\mathrm{host}} = 4.44$ and $\sigma_{\mathrm{host}} = 0.9$ in natural log space are the best-fit values from K. Shin et al. (2023).
5. We take $P(\mathrm{DM}_{\mathrm{MW}})$ to be the convolution of $P(\mathrm{DM}_{\mathrm{MW,ISM}})$ and $P(\mathrm{DM}_{\mathrm{MW,halo}})$, as implemented by J. M. Cordes et al. (2022). A $\mathrm{DM}_{\mathrm{MW,ISM}}$ estimate is obtained for each FRB using the NE2001 model for DM in the MW ISM (J. M. Cordes & T. J. W. Lazio 2002) and the Galactic coordinates of the FRB. To account for uncertainties in the NE2001 model (D. H. F. M. Schnitzeler 2012), $P(\mathrm{DM}_{\mathrm{MW,ISM}})$ is taken to be a flat distribution with a 40% spread centered on the NE2001 value. $P(\mathrm{DM}_{\mathrm{MW,halo}})$ is a flat distribution from 25–80 $\mathrm{pc\,cm^{-3}}$, incorporating the various estimates for $\mathrm{DM}_{\mathrm{MW,halo}}$ (J. X. Prochaska & Y. Zheng 2019; S. Yamasaki & T. Totani 2020; A. M. Cook et al. 2023; K. Shin et al. 2023).

[21] https://github.com/FRBs/FRB/blob/main/frb/dm/prob_dmz.py

6. For each z in $P(z|\mathrm{DM})$, the corresponding energy can be calculated as :

$$E_{\mathrm{iso}}(z) = \frac{4\pi D_{\mathrm{L}}^2}{(1+z)^{2+\alpha}} F_\nu \Delta\nu, \tag{8}$$

where $\mathrm{D_L}$ is the luminosity distance, F_ν is the fluence, $\Delta\nu$ is the intrinsic bandwidth, and α is the spectral index of the FRB. The FRB signal is integrated in the band-averaged time series to obtain the fluence, assuming $\alpha = 0$. We carry this assumption forward in the energy calculation as well, where $\alpha = 0$ essentially implies that the energies are referenced at the rest-frame frequency. Additionally, to be consistent with other works (C. W. James et al. 2022; K. Shin et al. 2023), we assume an intrinsic bandwidth of 1 GHz for FRB sources. Using change of variables for $P(z|\mathrm{DM})$, we obtain

$$\begin{aligned} P(E_{\mathrm{iso}}|\mathrm{DM}) &= P(z|\mathrm{DM}) \left| \frac{dz}{dE_{\mathrm{iso}}} \right| \\ &= P(z|\mathrm{DM}) \frac{D_{\mathrm{L}} H_0 \sqrt{\Omega_m (1+z)^3 + \Omega_\Lambda}}{2E_{\mathrm{iso}}(1+z)c}, \end{aligned} \tag{9}$$

where $c = 3 \times 10^8\ \mathrm{m\ s^{-1}}$ is the speed of light. A detailed derivation for this form of $P(E_{\mathrm{iso}}|\mathrm{DM})$ is presented in Appendix B.

A lower limit on $E_{\mathrm{iso}}^{\mathrm{max}}$ is then estimated jointly from $P(E_{\mathrm{iso}}|\mathrm{DM})$ for each FRB in the sample. To do so, we evaluate the probability that at least one FRB in the sample has an energy above a trial energy (E_{trial}) as:

$$P(E_{\mathrm{iso}} > E_{\mathrm{trial}}) = 1 - \prod_{i=1}^{N} P(E_{\mathrm{iso}} < E_{\mathrm{trial}}|\mathrm{DM})_{\mathrm{FRB}\,i} \tag{10}$$

where $P(E_{\mathrm{iso}} < E_{\mathrm{trial}}|\mathrm{DM})_{\mathrm{FRB}\,i}$ is the cumulative distribution function (CDF) associated with $P(E_{\mathrm{iso}}|\mathrm{DM})$ for FRB i, and N is the number of FRBs in the sample. For a given sample of bursts, E_{trial} ranges between the minimum possible energy, obtained using the minimum FRB fluence in the sample and $z = 0.01$, and the maximum possible energy, obtained using the maximum FRB fluence in the sample and $z = 6$. $P(E_{\mathrm{iso}} > E_{\mathrm{trial}})$ is calculated for each E_{trial}. The maximum E_{trial} value with $P(E_{\mathrm{iso}} > E_{\mathrm{trial}}) > 0.99$ is considered to be our estimate for the lower limit on $E_{\mathrm{iso}}^{\mathrm{max}}$. This a "lower limit" because, according to the method described above, there is a $\gtrsim$99% chance that there is at least 1 FRB in the sample with energy higher than this value.

3.2. Simulations to Verify the Framework

To verify the robustness of the framework described in Section 3.1, we apply it to simulated FRB samples and validate the obtained lower limit on $E_{\mathrm{iso}}^{\mathrm{max}}$ against the true $E_{\mathrm{iso}}^{\mathrm{max}}$ in the sample. The simulated FRB samples are generated in the following way:

1. We assume a Schechter function for the FRB energy distribution, with power-law index γ and an exponential energy cutoff at $E_{\mathrm{iso}}^{\mathrm{cutoff}}$ at the high-energy end. We assume $\mathrm{DM_{host}}$ to be a log-normal distribution with mean μ_{host} and standard deviation σ_{host}, as in Equation (7).
2. We generate simulated samples using combinations of the 95% confidence interval values for $E_{\mathrm{iso}}^{\mathrm{cutoff}}$, γ, μ_{host}, and σ_{host}, obtained from the posterior probability distributions from K. Shin et al. (2023). These parameter values were chosen so that our framework can be tested for simulations covering the extreme case scenarios for the $\mathrm{DM_{host}}$ distribution and FRB energy function. We thus obtain 16 different simulated samples as specified in Table 1. Additionally, we obtain a simulated sample for the best-fit parameter values from K. Shin et al. (2023).
3. For each FRB in a simulated sample, we draw z and extragalactic DM, $\mathrm{DM_{exg}} = \mathrm{DM_{cosmic}} + \mathrm{DM_{host}}$, from the joint probability distribution of z and DM, $P(\mathrm{DM}, z)$, obtained using the zDM package (C. W. James et al. 2022), assuming population and survey parameters as specified in K. Shin et al. (2023), but varying $E_{\mathrm{iso}}^{\mathrm{cutoff}}$, γ, μ_{host}, and σ_{host} to the combinations in Table 1.
4. For each FRB in a simulated sample, we draw an energy value from the corresponding Schechter function such that the obtained fluence is >3.5 Jy ms, the median 95% fluence threshold of Catalog 2 FRBs (CHIME/FRB Collaboration et al. 2026).
5. We take each of $\mathrm{DM_{MW,\ ISM}}$ and $\mathrm{DM_{MW,\ halo}}$ to be 50 pc cm^{-3}. The total DM is then given by Equation (1).
6. The maximum extragalactic DM in the subsample of Catalog 2 FRBs used in this work is 3167 pc cm^{-3}. For each simulated sample, we randomly choose a maximum extragalactic DM value between 3000 and 3334 pc cm^{-3}, since this range is symmetric about the observed value. We then only select simulated FRBs that have extragalactic DM >100 and less than or equal to the maximum extragalactic DM value corresponding to a given simulated sample. This ensures that the simulated FRBs cover a similar range of extragalactic DMs as the Catalog 2 FRBs. We, thus, obtain simulated samples of size $N = 2998$ FRBs each, equal to the size of the real FRB sample we have.

An example of the framework applied to a simulated FRB sample is shown in Figure 1(a). The $P(E_{\mathrm{iso}} > E_{\mathrm{trial}})$ (gray curve) is equal to 1 up to a certain E_{trial}, because for these E_{trial} values, there is a 100% chance that at least one FRB in the sample has a higher energy. The maximum E_{trial} where $P(E_{\mathrm{iso}} > E_{\mathrm{trial}}) > 0.99$ is our estimate for the lower limit on $E_{\mathrm{iso}}^{\mathrm{max}}$ (blue dashed line), which is also where $P(E_{\mathrm{iso}} > E_{\mathrm{trial}})$ starts falling rapidly before dropping to 0. The lower limit on $E_{\mathrm{iso}}^{\mathrm{max}}$ is slightly higher than the true maximum FRB energy (black dashed line) sampled from the Schechter function with cutoff energy $E_{\mathrm{iso}}^{\mathrm{cutoff}}$ (red dashed line) for this simulated sample. This is because, in some cases, it is possible for an FRB to have large DM contributions from the host galaxy or intervening galaxy halos such that the $P(z|\mathrm{DM})$ favors a larger z than the true z of the FRB. These FRBs can falsely seem more energetic than they truly are. In Section 3.3, we develop a method to use the simulated samples to estimate the number of such outliers, which we then remove from the Catalog 2 sample to obtain a realistic value for the lower limit on $E_{\mathrm{iso}}^{\mathrm{max}}$.

Table 1
Results of the Framework Applied on Simulated FRB Samples and the Catalog 2 FRB Sample

$\mu_{\rm host}$	$\sigma_{\rm host}$	$\log_{10}(E_{\rm iso}^{\rm cutoff})$ (erg)	γ	No. of Outliers	Simulated Sample: $\log_{10}$(True $E_{\rm iso}^{\rm max}$) (erg)	Simulated Sample: $\log_{10}$(Lower Limit on $E_{\rm iso}^{\rm max}$) (erg)	Catalog 2: $\log_{10}$(Lower Limit on $E_{\rm iso}^{\rm max}$) (erg)
1.93	**0.41**	**41.38**	**−1.30**	**7**	**42.15**	**42.14**	**42.17**
1.34	0.08	40.40	−2.04	64	40.96	40.96	41.94
1.34	0.08	40.40	0.99	239	41.42	41.41	41.68
1.34	0.08	42.46	−2.04	5	42.71	42.60	42.19
1.34	0.08	42.46	0.99	20	43.46	43.44	42.08
1.34	0.82	40.40	−2.04	334	40.87	40.86	41.63
1.34	0.82	40.40	0.99	498	41.44	41.43	41.49
1.34	0.82	42.46	−2.04	4	42.69	42.56	42.20
1.34	0.82	42.46	0.99	22	43.52	43.52	42.07
2.40	0.08	40.40	−2.04	555	40.83	40.83	41.47
2.40	0.08	40.40	0.99	1236	41.42	41.42	41.09
2.40	0.08	42.46	−2.04	0	42.99	42.96	42.28
2.40	0.08	42.46	0.99	55	43.47	43.46	41.96
2.40	0.82	40.40	−2.04	1129	40.85	40.84	41.15
2.40	0.82	40.40	0.99	1322	41.43	41.43	41.05
2.40	0.82	42.46	−2.04	2	43.09	42.78	42.24
2.40	0.82	42.46	0.99	78	43.54	43.54	41.92

Note. $\mu_{\rm host}$ and $\sigma_{\rm host}$ are in $\log_{10}$ space and describe the mean and standard deviation for the log-normal distribution for $\rm DM_{host}$, $E_{\rm iso}^{\rm cutoff}$ describes the cutoff energy, and γ describes the power-law index of the Schechter function used in each simulation. The lower limit on $E_{\rm iso}^{\rm max}$ for the simulated samples is obtained after removing the corresponding number of outliers and is consistent with the true $E_{\rm iso}^{\rm max}$ in the sample. For Catalog 2 FRBs, the lower limit on $E_{\rm iso}^{\rm max}$ is obtained after removing outliers and multiplying the median increase factor between the baseband fluences and lower limits on fluences. The simulated sample obtained using the best-fit parameter values from K. Shin et al. (2023) and the resulting best estimate for the lower limit on $E_{\rm iso}^{\rm max}$ are marked in bold.

3.3. Removing Outliers

To constrain the maximum energy of FRBs, we must exclude FRBs for which $P(E_{\rm iso}|{\rm DM})$ favors a higher energy than their true energy due to larger than expected $\rm DM_{host}$ and/or $\rm DM_{cosmic}$. In the absence of known z for most Catalog 2 FRBs, it is not possible to identify which FRBs are affected by this issue. Since we don't know which FRBs need to be removed from the Catalog 2 sample, we use the simulated samples to inform the number of FRBs that need to be removed.

To do so, we find the median energies inferred from $P(E_{\rm iso}|{\rm DM})$ for each FRB in a simulated sample. The FRBs that have the highest inferred energies affect the lower limit on $E_{\rm iso}^{\rm max}$ estimate the most. Thus, we remove the highest inferred energy FRBs from the simulated samples until the lower limit on $E_{\rm iso}^{\rm max}$ obtained from the remaining FRBs is less than or equal to the true $E_{\rm iso}^{\rm max}$ in the sample. The FRBs that are removed are considered outliers. An example of this process is shown in Figure 1 for a simulated sample. The lower limit on $E_{\rm iso}^{\rm max}$ (blue dashed line) obtained in Figure 1(a) before removing the outliers is greater than the true $E_{\rm iso}^{\rm max}$ (black dashed line). Figure 1(b) shows the median inferred energy with 68% confidence interval plotted against the true energies of the FRBs in the simulated sample. The black line shows where the true and inferred energies are equal. The FRBs with the highest inferred energies that are considered outliers (red points) are all below the black line, having inferred energies greater than the true energies. The lower limit on $E_{\rm iso}^{\rm max}$ (blue dashed line) obtained in Figure 1(c) after removing the outliers is consistent and overlaps with the true $E_{\rm iso}^{\rm max}$ (black dashed line) in the simulated sample. We similarly obtain the number of outliers to be removed for all of our simulated samples. For different assumptions of $\rm DM_{host}$ distribution and energy function of FRBs, this method allows us to estimate the number of contaminants with the highest inferred energies that need to be removed in order to obtain a realistic value for the lower limit on $E_{\rm iso}^{\rm max}$ from Catalog 2 FRBs. The number of outliers and the lower limit on $E_{\rm iso}^{\rm max}$ obtained from the simulated samples and Catalog 2 FRBs are discussed in Section 4.

4. Results

In Table 1 we present the lower limit on $E_{\rm iso}^{\rm max}$ from Catalog 2 FRBs after removing the highest inferred energy data points as outliers, where the number of outliers is informed from the 17 simulated samples with different $\rm DM_{host}$ distributions and FRB energy functions. Our estimate for the lower limit on $E_{\rm iso}^{\rm max}$ ranges between 1.1×10^{41}–1.9×10^{42} erg. This is better visualized in Figure 2, which shows how the lower limit on $E_{\rm iso}^{\rm max}$ varies as a function of the number of outliers removed. Our best estimate for the lower limit on $E_{\rm iso}^{\rm max}$ is 1.5×10^{42} erg, obtained after removing the number of outliers informed from the simulated sample generated using the best-fit $\rm DM_{host}$ and energy distributions from K. Shin et al. (2023).

For the 17 simulated samples, the number of outliers range between 0 and 1322. The outlier removal method ensures that the lower limit on $E_{\rm iso}^{\rm max}$ for these simulated samples is consistent with the true value in the sample as shown in Table 1. It is clear that this lower limit is dependent on the assumed FRB luminosity function. Higher $E_{\rm iso}^{\rm cutoff}$ and γ give simulated FRBs with higher energies, leading to higher values for the lower limit on $E_{\rm iso}^{\rm max}$. Moreover, the number of outliers is also sensitive to the assumed FRB luminosity function, such that simulations with $\gamma = 0.99$ have the highest number of outliers. Such a γ allows for more FRBs to have energies close to the true $E_{\rm iso}^{\rm max}$ in the sample, such that only a small excess DM from the host or intervening halos is required to push their inferred energies above the true $E_{\rm iso}^{\rm max}$. On the contrary, the

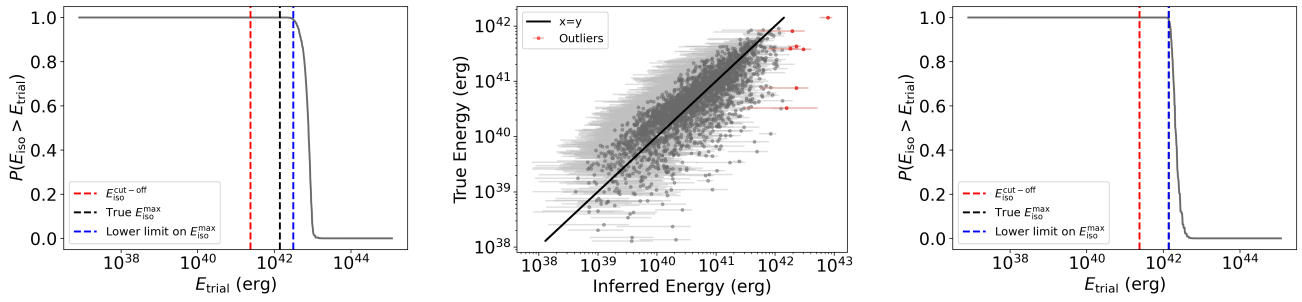

(a) (b) (c)

Figure 1. For the simulated FRB sample having the best-fit values of μ_{host}, σ_{host}, E_{iso}^{cutoff}, and γ from K. Shin et al. (2023), panel (a) shows $P(E_{iso} > E_{trial})$ (gray line) before removing the outliers. The lower limit on E_{iso}^{max} (blue dashed line) is slightly higher than the true E_{iso}^{max} (black dashed line). Panel (b) shows the median inferred energies with 68% confidence interval from $P(E_{iso}|DM)$ for the simulated FRBs plotted against their true energies. The black line shows where the inferred and true energies are equal. The highest inferred energy FRBs, which are considered outliers, are marked in red. Panel (c) shows $P(E_{iso} > E_{trial})$ (gray line) after removing the outliers. The lower limit on E_{iso}^{max} (blue dashed line) in this case is consistent and overlaps with the true E_{iso}^{max} (black dashed line). As expected, the lower limit on E_{iso}^{max} is higher than the Schechter function cutoff energy E_{iso}^{cutoff} (red dashed line). This describes our method of obtaining a realistic value for the lower limit on E_{iso}^{max} for a simulated sample after removing a subsample of highest inferred energy bursts as outliers.

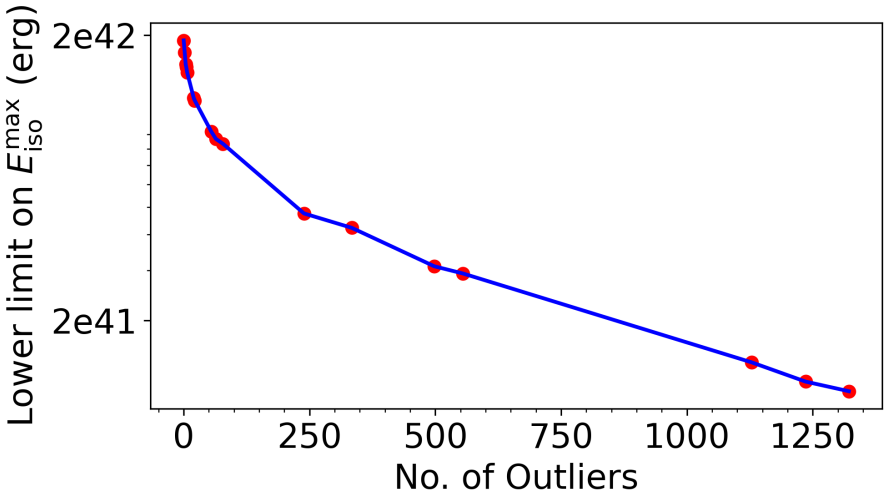

Figure 2. The lower limit on E_{iso}^{max} from Catalog 2 FRBs as a function of the number of highest inferred energy FRBs that are removed from the sample as outliers. The red points mark the lower-limit value for the number of outliers obtained from the 17 simulated FRB samples.

simulations with $\gamma = -2.04$ have the least number of outliers because there are very few FRBs with energies close to the true E_{iso}^{max}. Our results show that the number of outliers is also sensitive to the assumed DM_{host} distribution, such that simulations with larger values of μ_{host} and σ_{host} have a larger number of outliers.

Our framework applied to the simulated samples leads to a nonnegligible number of outliers in most cases, partly because of the broad range of E_{iso}^{cutoff}, γ, μ_{host}, and σ_{host} used to generate the simulated samples, and partly because no telescope-dependent selection effects are included in the framework. The number of outliers is, in fact, estimated to calibrate the framework to account for the selection effects. In Appendix C and Table C1, we explore a way of including the CHIME/FRB selection effects in the framework, where, instead of using a flat, uninformative prior for $P(z)$ in Equation (2), we use the best-fit distribution of observed redshifts by CHIME/FRB, $P_{obs}(z)$, from K. Shin et al. (2023). $P_{obs}(z)$ peaks at $z \sim 0.36$ and drops rapidly after that, hitting 0 for $z > 2$. As shown in Table C1, using $P_{obs}(z)$ leads to a reduction in the number of outliers for the simulated samples. However, samples with $\log_{10}(E_{iso}^{cutoff}) = 40.40$ still have a significant number of outliers. This is because, for this low value of E_{iso}^{cutoff}, the majority of the simulated FRBs have $DM_{exg} < 1000\,pc\,cm^{-3}$ and $z < 0.5$. Such a small range of observed z with the maximum allowed DMs up to $3334\,pc\,cm^{-3}$ will naturally produce more FRBs with significant excess DM compared to what is expected from Equation (4), leading to a large number of outliers. Moreover, $DM_{exg} < 1000\,pc\,cm^{-3}$ implies a z much lower than 2, such that $P_{obs}(z) = 0$ for $z > 2$ does not have any impact. This new framework applied on Catalog 2 FRBs leads to a similar lower limit on E_{iso}^{max} range of 1.1×10^{41}–1.6×10^{42} erg compared to the results in Table 1. The lower limit on E_{iso}^{max} estimate does not increase even for a lower number of outliers, because for this form of $P_{obs}(z)$, $P(z|DM)$ favors lower-z, and thus, $P(E_{iso}|DM)$ favors lower E_{iso}. For the rest of this work, we will refer to the results in Table 1 obtained using a flat, uninformative prior for $P(z)$ as our constraints on E_{iso}^{max}.

An important caveat in applying the framework described in Section 3.1 on Catalog 2 FRBs is that the fluences in Catalog 2 are lower limits calculated under the assumption that the FRBs

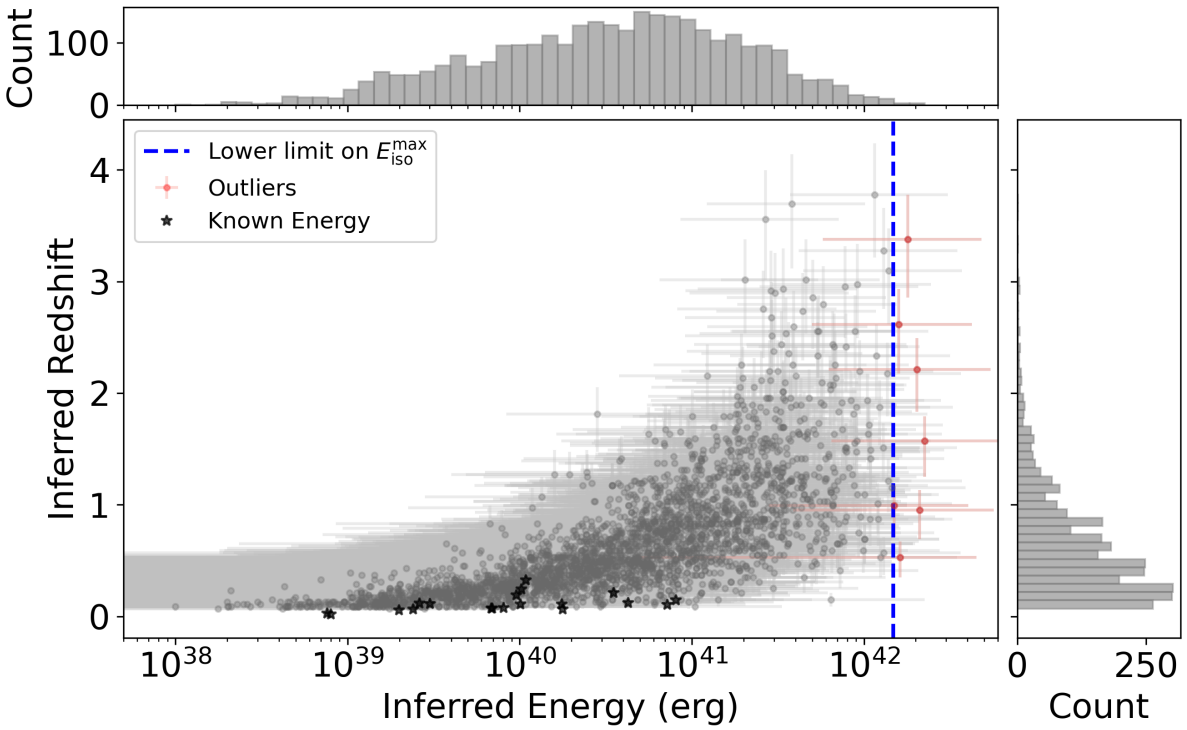

Figure 3. For the 2998 Catalog 2 FRBs, the median z and energy from $P(z|\mathrm{DM})$ and $P(E|\mathrm{DM})$, respectively, are plotted, along with the 68% confidence intervals. The red points show the 19 outliers that were removed for our best estimate of the lower limit on $E_{\mathrm{iso}}^{\mathrm{max}}$ of 1.5×10^{42} erg (see Table 1), which is shown by the vertical blue dashed line. The black stars mark the 19 FRBs that have confident hosts with known z and robust energy measurements, enabled by localizations with the CHIME–KKO baseline. Irrespective of the inferred z, the inferred energies of the FRBs appear collectively limited around $\sim 10^{42}$ erg.

are detected at the location of the highest sensitivity within CHIME's primary beam (B. C. Andersen et al. 2023). A subset of these FRBs has baseband voltage data and, thus, more precise localizations, allowing for the use of the accurate location of FRBs within the primary beam to estimate fluence values rather than lower limits (CHIME/FRB Collaboration et al. 2024). The increase factor between the baseband fluences and the lower limits on fluence is dependent on where within the primary beam the FRBs are detected, and ranges between 1 and ∼300, with only ∼15% of bursts having increase factor >10. We estimate the lower limit on $E_{\mathrm{iso}}^{\mathrm{max}}$ for Catalog 2 FRBs using the lower limits on fluences and then multiplying the resulting value by the median increase factor of 3. We note that the simulations described in Section 3.2 generate actual fluences of FRBs, not lower limits on fluence, and thus, the lower limit on $E_{\mathrm{iso}}^{\mathrm{max}}$ for the simulated samples does not need to be multiplied by the increase factor.

In Figure 3, we show the median z and energy for the Catalog 2 FRBs from $P(z|\mathrm{DM})$ and $P(E_{\mathrm{iso}}|\mathrm{DM})$, respectively, along with their 68% confidence intervals. The increase factor is taken into account while calculating the energy and error bars on energy. The vertical blue dashed line shows our best estimate for the lower limit on $E_{\mathrm{iso}}^{\mathrm{max}}$ of 1.5×10^{42} erg from Catalog 2 FRBs, after removing 19 outliers (red points). Additionally, the black stars show the z and energies of 19 FRBs with confident host associations that were localized using interferometry between CHIME and the KKO Outrigger (A. E. Lanman et al. 2024; CHIME/FRB Collaboration et al. 2025a). These local-Universe FRBs with relatively low z agree with the low-energy end of the inferred redshift-energy distribution for Catalog 2 FRBs. An interesting observation in Figure 3 is the turnover of the z-energy data points at higher energies such that, irrespective of the inferred z, the inferred energies do not go far beyond $\sim 10^{42}$ erg, which is in agreement with our best estimate for the lower limit on $E_{\mathrm{iso}}^{\mathrm{max}}$. This suggests that we are already probing the maximum energy of FRBs using the available sample of FRBs.

An important consideration in such an analysis is the selection biases introduced by the instrument. For example, K. Shin et al. (2023) showed that for CHIME/FRB, there is a "turnover" in the DM-z relationship above $\mathrm{DM} \sim 2000\,\mathrm{pc\,cm^{-3}}$ such that the Macquart relationship is no longer valid. Such FRBs are more likely to occur at $z < 2$, rather than at $z > 2$, as expected from the Macquart relation. The effect of this on our lower limit on $E_{\mathrm{iso}}^{\mathrm{max}}$ estimate from Catalog 2 FRBs is taken into account by removing outliers. The FRBs in the simulated sample that have z inferred from $P(z|\mathrm{DM})$ larger than the true value, and that falsely inflate the lower limit on $E_{\mathrm{iso}}^{\mathrm{max}}$ value, are considered outliers. Our method estimates the number of such outliers, which are then removed from the Catalog 2 sample before estimating the lower limit on $E_{\mathrm{iso}}^{\mathrm{max}}$. Another way to deal with this selection effect could be removing all FRBs having $\mathrm{DM} > 2000\,\mathrm{pc\,cm^{-3}}$ from the Catalog 2 sample before obtaining the lower limit on $E_{\mathrm{iso}}^{\mathrm{max}}$. Doing so, we obtain a lower limit on $E_{\mathrm{iso}}^{\mathrm{max}}$ of 1.7×10^{42} erg. This is consistent with the higher end of the range of values we obtained in Table 1. This is because removing FRBs with $\mathrm{DM} > 2000\,\mathrm{pc\,cm^{-3}}$ would exclude the FRBs with the highest inferred z. However, as seen from Figure 3, there are FRBs with relatively lower inferred z that have the highest inferred energies. Thus, our outlier removal method presents a more conservative range of values for the lower limit on $E_{\mathrm{iso}}^{\mathrm{max}}$.

Moreover, to ensure that we are not missing out on the highest-energy bursts due to CHIME/FRB's selection bias

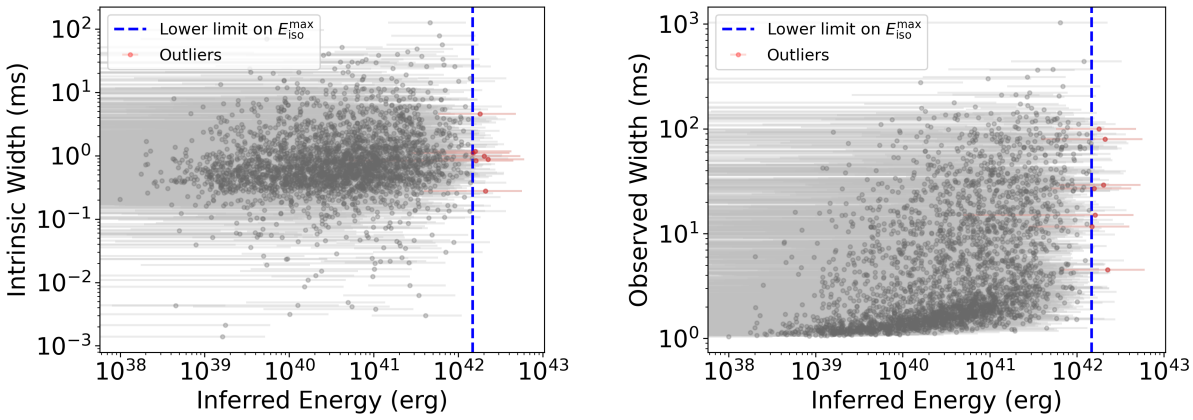

Figure 4. The median inferred energies with 68% confidence interval as a function of the intrinsic widths (left panel) and observed widths (right panel) of Catalog 2 FRBs. The red points mark the 19 outliers that were removed to obtain our best estimate for the lower limit on E_{iso}^{max} (blue dashed line). There appears to be no strong correlation between the energies and widths of the highest inferred energy FRBs.

against wider bursts, we plot the median inferred energies with 68% confidence interval as a function of the intrinsic widths and observed widths of Catalog 2 FRBs in Figure 4. CHIME/FRB Collaboration et al. (2026) presented the intrinsic width estimates for the FRBs, and we obtain the observed widths by adding the intrinsic widths, intrachannel DM smearing, scattering timescale, and the time resolution of the data in quadrature (E. Fonseca et al. 2024). In Figure 4(a), it is clear that there is no strong correlation between the intrinsic widths and inferred energies of the FRBs, with the Pearson correlation coefficient[22] being 0.08. In Figure 4(b), there is a positive correlation between the observed widths and inferred energies due to the lack of high-width and low-energy data points. The Pearson correlation coefficient in this case is 0.27. The deficit of data points at the low-energy end is an observational bias due to the difficulty in detecting faint bursts that are wider. On the other hand, bursts with the highest inferred energies span the entire range of observed width values. To eliminate the bias at the low-energy end, we calculate the Pearson correlation coefficient for bursts with inferred energies $>10^{40}$ erg, and we obtain a value of 0.09. Thus, our results do not seem affected by the detection biases of CHIME/FRB.

5. Discussion

The maximum energy of FRBs can be an important indicator of the energy reservoir of FRB sources and, thus, provides crucial insights into their origins. We, therefore, compare our best estimate for the lower limit on E_{iso}^{max} of $\sim 10^{42}$ erg with other works studying FRB energetics, and discuss the resulting implications for FRB progenitors and emission mechanisms.

5.1. Comparison to Other Works

Various works have studied the energetics of FRBs by modeling the FRB energy distribution with a Schechter function. The motivation to use this functional form is to allow for FRBs with energies higher than E_{iso}^{cutoff}, but with orders-of-magnitude lower rates. Similar to the lower limit on E_{iso}^{max}, E_{iso}^{cutoff} is not equal to but is close to E_{iso}^{max}. These other works use FRBs detected at different radio frequencies and with different observing bandwidths. Under our previously stated assumptions of $\alpha = 0$ and $\Delta\nu = 1$ GHz, we compare E_{iso}^{cutoff} obtained in these works with our lower limit on E_{iso}^{max}.

R. Luo et al. (2020a) used 46 FRBs detected with various instruments, including the upgraded Molonglo Observatory Synthesis Telescope in the Southern-Sky survey (UTMOST-SS; M. Caleb et al. 2017) and Australian Square Kilometre Array Pathfinder in the Commensal Real-time ASKAP Fast Transient survey (ASKAP/CRAFT; R. M. Shannon et al. 2018), taking into account their selection biases and found $\log_{10} E_{iso}^{cutoff} = 42.08^{+0.3}_{-0.06}$ erg. C. W. James et al. (2022) used 16 ASKAP/CRAFT FRBs localized to their host galaxies and 60 poorly localized FRBs with no known hosts from Parkes and ASKAP/CRAFT and found $\log_{10} E_{iso}^{cutoff} = 41.26^{+0.27}_{-0.22}$ erg. K. Shin et al. (2023) used 225 FRBs presented in the First CHIME/FRB Catalog (CHIME/FRB Collaboration et al. 2021) calibrated for selection effects and found $\log_{10} E_{iso}^{cutoff} = 41.38^{+0.51}_{-0.51}$ erg. W. R. Arcus et al. (2025) used 63 FRBs detected by ASKAP, including 28 FRBs with known redshifts, accounting for cosmological and instrumental effects, and found $\log_{10} E_{iso}^{cutoff} = 41.80 \pm 0.39$ erg. While these works have studied the energy function of a population of one-off FRBs, another approach is to use bursts from individual repeating FRB sources. O. S. Ould-Boukattine et al. (2024) observed the repeating FRB 20220912A for 1500 hr and detected 130 high-energy bursts having $\log_{10} E_{iso}^{cutoff}$ of $41.32^{+0.45}_{-0.30}$ erg. Using a $>10\times$ larger sample than previous studies, the $\log_{10}$ (lower limit on E_{iso}^{max}) range of 41.05–42.28 erg obtained in this work and presented in Table 1 is consistent, within error bars, with the $\log_{10} E_{iso}^{cutoff}$ obtained in other works. While such a large sample of FRBs should present tight constraints on the maximum energy of FRBs, we note that our outlier removal method assumes a broad range of μ_{host}, σ_{host}, E_{iso}^{cutoff}, and γ values, leading to a conservative estimate for the lower limit on E_{iso}^{max}. In the regime where a large sample of FRBs have known redshifts, such an outlier removal process won't be necessary, leading to much smaller uncertainties on the maximum energy of FRBs.

[22] A Pearson correlation coefficient evaluates the strength of a linear relationship between two variables. Its value can range between −1 and 1, with −1 indicating a perfect negative correlation, and +1 indicating a perfect positive correlation. Values close to 0 indicate no correlation.

In addition to these FRB population studies, there have also been studies where individual high-energy bursts from one-off and repeating FRBs have been reported.[23] V. Ravi et al. (2019) reported a burst detected and localized using the Deep Synoptic Array (DSA) having $\log_{10} E_{\rm iso} = 42.75$ erg. S. D. Ryder et al. (2023) presented an FRB originating at $z = 1$ detected by ASKAP/CRAFT with $\log_{10} E_{\rm iso} = 42.30$ erg. In terms of repeating FRBs, in the sample of high-energy bursts from FRB 20201124A presented in F. Kirsten et al. (2024), the highest-energy burst has $\log_{10} E_{\rm iso} = 41.49$ erg. The $\log_{10}$ (lower limit on $E_{\rm iso}^{\rm max}$) obtained from Catalog 2 FRBs is, thus, similar to the energies of highly energetic one-off and repeating FRBs presented in other works.

5.2. Implications for the Emission Mechanisms and Progenitors of FRBs

In this work, we study the largest sample of one-off FRBs containing 2998 unique sources to constrain $E_{\rm iso}^{\rm max}$. It is informative that the range of lower limit on $E_{\rm iso}^{\rm max}$ that we obtain in this work is consistent with the various studies of FRB energetics done using FRBs detected with different instruments with their own intrinsic selection effects. This suggests there is a limit to the amount of energy that FRB sources can produce. This is also apparent in Figure 3, where the inferred energies do not go far beyond $\sim 10^{42}$ erg, even for FRBs with high inferred z, providing further indication of the energy reservoir of FRB sources.

Assuming the radio efficiency factor for FRB sources to be $\eta_{\rm radio} \lesssim 10^{-4}$ based on the ratio of energies released in the radio and X-ray bursts from the Galactic magnetar SGR 1935 +2154 (C. D. Bochenek et al. 2020), and adopting similar beaming fractions for radio and high-energy emission, this gives an isotropic equivalent source energy of $E_{\rm iso}^{\rm src} \gtrsim 10^{46}$ erg. The total external dipolar magnetic energy of a magnetar is estimated to be $E_{dip} = 1/6 B_P^2 R^3 = (1.7 \times 10^{47}\ {\rm erg}) B_{P,15}^2 R_6^3$ for a surface dipole magnetic field strength of $B_P = 10^{15}$ G and a neutron-star radius of $R = 10^6$ cm. It is also possible for a magnetar to have local regions of higher magnetic field strengths from multipolar field components (V. M. Kaspi & A. M. Beloborodov 2017). Thus, magnetars have the required energy reservoir to power such energetic FRBs. This is further proven by the fact that the most energetic magnetar giant flares ever observed have isotropic equivalent energies ranging over 10^{46}–10^{47} erg (K. Hurley et al. 2005; E. O. Ofek et al. 2006). In terms of FRB emission mechanisms, the most energetic FRBs could be produced via synchrotron maser emission at forward shocks when extremely energetic magnetar giant flares collide with the surrounding medium (B. D. Metzger et al. 2019). On the other hand, P. Kumar et al. (2017) estimated a beaming-corrected energy release of $\sim 10^{36}$ erg in emission mechanisms involving reconnection of magnetic fields in the magnetosphere of magnetars. If the most energetic FRBs are produced via reconnection in the magnetosphere, this suggests an FRB beaming fraction of $\sim 10^{-6}$. Alternatively, this could imply that low- and high-energy bursts are produced by reconnection in magnetosphere and synchrotron maser emission, respectively.

[23] For works in which spectral energy has been reported, we assume an intrinsic bandwidth of 1 GHz for the FRB to obtain their energies.

Another interesting observation from Section 5.1 is that one-off FRBs and bursts from repeating FRB sources have similar maximum energies. This could imply that one-off and repeating FRB sources have the same energy reservoir, which may suggest a common progenitor, but possibly different emission mechanisms, given observed differences in burst morphologies of one-off and repeat bursts (Z. Pleunis et al. 2021; A. P. Curtin et al. 2025). A common progenitor scenario is also consistent with the conclusions from F. Kirsten et al. (2024), O. S. Ould-Boukattine et al. (2024), and W.-P. Sun et al. (2026) that one-off FRBs could be the highest-energy bursts from repeating sources that appear as one-offs due to their lower rates.

The energy reservoir of FRB sources is also revealed by the sum total of energy of repeat bursts. J.-S. Zhang et al. (2025) observed 11,553 bursts from the hyperactive repeating source FRB 20240114A with isotropic energies ranging over 10^{37}–10^{40} erg, assuming an intrinsic burst bandwidth of 1 GHz. The total energy of all bursts combined is 2.5×10^{42} erg, similar to that of the most energetic one-off FRBs. FRB sources can, thus, produce thousands of low-energy bursts releasing the same amount of energy as a single high-energy burst, similar to hundreds of X-ray bursts observed during magnetar burst storms producing the same amount of energy as a single very energetic flare (G. Younes et al. 2020; C.-P. Hu et al. 2025). On the other hand, O. S. Ould-Boukattine et al. (2024) observed 130 high-energy bursts from FRB 20220912A having total isotropic energy of 1.3×10^{43} erg. An explanation for such high energies could be that the magnetic field powering the repeat bursts is replenished over the activity period of the repeater. If a one-off FRB with energy 10^{43}–10^{44} erg is observed where replenishment cannot occur, it could imply unusually high $\eta_{\rm radio}$ and/or B_P, or extremely beamed emission such that $E^{\rm src}$ is still within what a typical magnetar could produce (D. Li & U.-L. Pen 2024). Thus, such highly energetic bursts, if detected, would provide stringent constraints on the parameters in FRB emission mechanism models involving magnetar progenitors. Alternatively, such bursts, whose nondetection points toward a very low rate of occurrence, could possibly originate from a different progenitor altogether.

5.3. FRB Energetics in the Era of CHIME/FRB Outriggers

The accurate estimation of FRB energies requires their z to be known. While in this work we combined the DMs and fluences of 2998 FRBs to estimate a lower bound on $E_{\rm iso}^{\rm max}$, knowing the z and, thus, the energies for such a large sample of FRBs would either confirm that there is a limit of $\sim 10^{42}$ erg for the most energetic FRBs, or reveal the presence of even more energetic bursts. Moreover, as discussed in Section 5.1, studies with even a small subsample of <100 FRBs with known z have led to tighter constraints on the energy distribution of FRBs.

CHIME/FRB's FRB detection rate of ~3 FRBs per day and its fluence threshold of ~3.5 Jy ms means that it detects many FRBs at relatively higher energies compared to other telescopes. The CHIME/FRB Outriggers, which are smaller CHIME-like telescopes forming a very-long-baseline interferometry network with CHIME, provide an FRB localization accuracy of $\sim 50 \times 100$ mas (CHIME/FRB Collaboration et al. 2025b) and will enable a z determination for many of these FRBs. Such a precise localization can also identify the local environments of FRBs within their host galaxies (CHIME/FRB Collaboration et al. 2025c). This opens up the

possibility of studying not just the burst properties, but also the locations of highly energetic FRBs, shedding more light on their progenitors and emission mechanisms. A distribution of FRB energies and their local environments could be useful to identify the existence of progenitor(s) that create extremely rare but much more energetic bursts than typical FRBs. The era of CHIME/FRB Outriggers is, thus, going to be game changing for identifying the most energetic FRBs and using them to understand the origins of FRBs.

6. Summary and Conclusion

The Second CHIME/FRB Catalog presents the largest currently available sample of FRBs along with their burst morphology parameters, including DMs and lower limits on fluence. We use 2998 one-off FRBs from this sample and develop a framework to combine their DMs and fluences with $P(z|\mathrm{DM})$ to obtain a lower limit on the maximum energy of FRBs. In order to verify the robustness of this framework, we generate 17 simulated FRB samples assuming different parameter values in the Schechter function for the FRB energy function and the log-normal distribution for $\mathrm{DM_{host}}$. Applying our framework on these simulated samples allows us to identify the number of outliers, which are FRBs that have large DM contributions from the host galaxy and/or intervening galaxy halos, which when removed, give us a lower limit on $E_{\mathrm{iso}}^{\mathrm{max}}$ consistent with the true $E_{\mathrm{iso}}^{\mathrm{max}}$ in the sample. The lower limit on $E_{\mathrm{iso}}^{\mathrm{max}}$ for the Catalog 2 sample, obtained after removing the number of outliers corresponding to the 17 simulated samples, ranges between 1.1×10^{41} and 1.9×10^{42} erg, with our best estimate being 1.5×10^{42} erg. Moreover, inferring the z and E_{iso} from $P(z|\mathrm{DM})$ and $P(E_{\mathrm{iso}}|\mathrm{DM})$, respectively, reveals that irrespective of the inferred z, the inferred energies of Catalog 2 FRBs are collectively limited around $\sim 10^{42}$ erg.

Our constraint on $E_{\mathrm{iso}}^{\mathrm{max}}$ is consistent with those obtained from other works involving much smaller populations of one-off FRBs, repeat bursts from repeating FRBs, and individual highly energetic FRBs. This agreement between our work, based on, by far, the largest available statistical sample, and various studies of FRB energetics involving FRBs detected with different instruments with their own intrinsic selection effects, might imply that current observations are able to probe the maximum energy achievable by FRBs. Moreover, similar maximum energy estimates between one-off and repeating FRBs might imply a common progenitor for these two populations of FRBs. It is also interesting that the amount of energy released by hyperactive repeating FRBs in hundreds to thousands of bursts can be released in an individual highly energetic burst. Under standard assumptions of radio efficiencies and dipolar magnetic fields, the most energetic FRBs are consistent with being produced from the most energetic magnetar giant flares; however, it is also reaching the limits of the amount of energy that magnetars could produce. Detecting bursts with energies an order of magnitude or more higher could imply extreme scenarios, such as an unusually large dipolar magnetic field, very small beaming fraction, or energy released from multipole field components for magnetar progenitors. It is also possible that such bursts, whose nondetection until now points toward a very low occurrence rate, come from a different progenitor altogether. CHIME/FRB and its Outriggers, with their excellent FRB detection rate and localization capability, will be instrumental in detecting the highest-energy FRBs and constraining their progenitor models and emission mechanisms.

Acknowledgments

We acknowledge that CHIME is located on the traditional, ancestral, and unceded territory of the Syilx/Okanagan people. We are grateful to the staff of the Dominion Radio Astrophysical Observatory, which is operated by the National Research Council of Canada. CHIME operations are funded by a grant from the NSERC Alliance Program and by support from McGill University, University of British Columbia, and University of Toronto. CHIME was funded by a grant from the Canada Foundation for Innovation (CFI) 2012 Leading Edge Fund (Project 31170) and by contributions from the provinces of British Columbia, Québec, and Ontario. The CHIME/FRB Project was funded by a grant from the CFI 2015 Innovation Fund (Project 33213) and by contributions from the provinces of British Columbia and Québec, and by the Dunlap Institute for Astronomy and Astrophysics at the University of Toronto. Additional support was provided by the Canadian Institute for Advanced Research (CIFAR), the Trottier Space Institute at McGill University, and the University of British Columbia. The CHIME/FRB baseband recording system is funded in part by a CFI John R. Evans Leaders Fund award to IHS.

The AstroFlash research group at McGill University, University of Amsterdam, ASTRON, and JIVE is supported by: a Canada Excellence Research Chair in Transient Astrophysics (CERC-2022-00009); an Advanced grant from the European Research Council (ERC) under the European Union's Horizon 2020 research and innovation program ("EuroFlash"; grant agreement No. 101098079); and an NWO-Vici grant ("AstroFlash"; VI.C.192.045).

V.S. is supported by a Fonds de Recherche du Quebec—Nature et Technologies (FRQNT) Doctoral Research Award. V.M.K. holds the Lorne Trottier Chair in Astrophysics & Cosmology, a Distinguished James McGill Professorship, and receives support from an NSERC Discovery grant (RGPIN 228738-13). K.W.M. is supported by NSF grant Nos. 2008031 and 2510771 and holds the Adam J. Burgasser Chair in Astrophysics. M.W.S is a Fonds de Recherche du Quebec—Nature et Technologies (FRQNT) postdoctoral fellow and acknowledges support from the Trottier Space Institute Fellowship program. A.P.C. is a Canadian SKA Scientist and is funded by the Government of Canada / est financé par le gouvernement du Canada. K.T.M is supported by an FRQNT Master's Research Scholarship. M.N. is a Fonds de Recherche du Quebec—Nature et Technologies (FRQNT) postdoctoral fellow. K.N. acknowledges support by NASA through the NASA Hubble Fellowship grant No. HST-HF2-51582.001-A awarded by the Space Telescope Science Institute, which is operated by the Association of Universities for Research in Astronomy, Incorporated, under NASA contract NAS5-26555. A.P. is a Trottier Space Institute Postdoctoral Fellow. A.B.P. acknowledges support by NASA through the NASA Hubble Fellowship grant HST-HF2-51584.001-A awarded by the Space Telescope Science Institute, which is operated by the Association of Universities for Research in Astronomy, Inc., under NASA contract NAS5-26555. A.B.P. also acknowledges prior support from a Banting Fellowship, a McGill Space Institute (MSI) Fellowship, and a Fonds de Recherche du Quebec—Nature et Technologies (FRQNT) Postdoctoral Fellowship.

Appendix A
Derivation of $P(\mathrm{DM}|z)$

Marginalizing over $\mathrm{DM_{MW}}$, $\mathrm{DM_{cosmic}}$, and $\mathrm{DM_{host}}$ and using the rules of conditional probability:

$$\begin{aligned} P(\mathrm{DM}|z) &= \int\int\int d\mathrm{DM_{MW}}\, d\mathrm{DM_{cosmic}}\, d\mathrm{DM_{host}} \\ &\quad \times P(\mathrm{DM}, \mathrm{DM_{MW}}, \mathrm{DM_{cosmic}}, \mathrm{DM_{host}}|z) \\ &\propto \int\int\int d\mathrm{DM_{MW}}\, d\mathrm{DM_{cosmic}}\, d\mathrm{DM_{host}} \\ &\quad \times P(\mathrm{DM}|\mathrm{DM_{MW}}, \mathrm{DM_{cosmic}}, \mathrm{DM_{host}}, z) \\ &\quad \times P(\mathrm{DM_{MW}}|\mathrm{DM_{cosmic}}, \mathrm{DM_{host}}, z) \\ &\quad \times P(\mathrm{DM_{cosmic}}|\mathrm{DM_{host}}, z)\, P(\mathrm{DM_{host}}|z). \end{aligned} \tag{A1}$$

Since the total DM of the FRB has to satisfy Equation (1), $P(\mathrm{DM}|\mathrm{DM_{MW}}, \mathrm{DM_{cosmic}}, \mathrm{DM_{host}}, z)$ becomes a delta function. $\mathrm{DM_{cosmic}}$ is dependent on z but not on any other DM components. $\mathrm{DM_{MW}}$ and $\mathrm{DM_{host}}$ are independent of other DM components, as well as z. Taking this into account, Equation (A1) becomes

$$\begin{aligned} P(\mathrm{DM}|z) \propto &\int\int d\mathrm{DM_{MW}}\, d\mathrm{DM_{cosmic}}\, d\mathrm{DM_{host}} \\ &\times \delta\left(\mathrm{DM} - \mathrm{DM_{cosmic}} - \mathrm{DM_{MW}} - \frac{\mathrm{DM_{host}}}{1+z}\right) P(\mathrm{DM_{MW}}) \\ &\times P(\mathrm{DM_{cosmic}}|z)\, P(\mathrm{DM_{host}}). \end{aligned} \tag{A2}$$

Integrating over $\mathrm{DM_{cosmic}}$ resolves the delta function and gives

$$\begin{aligned} P(\mathrm{DM}|z) \propto &\int\int d\mathrm{DM_{MW}}\, d\mathrm{DM_{host}} \\ &\times P(\mathrm{DM_{MW}})\, P\left(\mathrm{DM_{cosmic}} = \mathrm{DM} - \mathrm{DM_{MW}} \right. \\ &\left. - \frac{\mathrm{DM_{host}}}{1+z}|z\right) P(\mathrm{DM_{host}}). \end{aligned} \tag{A3}$$

Appendix B
Derivation of $P(E_{\mathrm{iso}}|\mathrm{DM})$

We start by using Equation (8) to derive $\left|\frac{dE_{\mathrm{iso}}}{dz}\right|$:

$$\frac{dE_{\mathrm{iso}}}{dz} = 4\pi F_\nu \Delta\nu \left(\frac{2\mathrm{D_L}}{(1+z)^2}\frac{d\mathrm{D_L}}{dz} - \frac{2\mathrm{D_L^2}}{(1+z)^3}\right). \tag{B1}$$

Under standard cosmology assumptions, the luminosity distance $\mathrm{D_L}$ depends on z as:

$$\mathrm{D_L}(z) = (1+z)\int_0^z \frac{c\, dz}{H_0\sqrt{\Omega_m(1+z)^3 + \Omega_\Lambda}}, \tag{B2}$$

such that

$$\frac{d\mathrm{D_L}}{dz} = \frac{\mathrm{D_L}}{1+z} + \frac{(1+z)c}{H_0\sqrt{\Omega_m(1+z)^3 + \Omega_\Lambda}}. \tag{B3}$$

Combining Equations (B1) and (B3) and substituting the $4\pi F_\nu \Delta\nu$ factor in terms of E_{iso}, we get:

$$\frac{dz}{dE_{\mathrm{iso}}} = \frac{1}{\frac{dE_{\mathrm{iso}}}{dz}} = \frac{\mathrm{D_L} H_0\sqrt{\Omega_m(1+z)^3 + \Omega_\Lambda}}{2E_{\mathrm{iso}}(1+z)c}. \tag{B4}$$

Substituting Equation (B4) in Equation (9) gives us $P(E_{\mathrm{iso}}|\mathrm{DM})$.

Appendix C
Lower Limit on $E_{\mathrm{iso}}^{\mathrm{max}}$ for a Telescope-dependent $P(z)$

In Table C1, we present the number of outliers and the lower limit on $E_{\mathrm{iso}}^{\mathrm{max}}$ obtained from the simulated samples and Catalog 2 FRBs assuming a telescope-dependent $P(z)$ for CHIME/FRB in Equation (2). The results obtained in this case are similar to that in Table 1.

Table C1
Results of the Framework Applied on Simulated FRB Samples and the Catalog 2 FRB Sample for a Telescope-dependent $P(z)$

μ_{host}	σ_{host}	$\log_{10}(E_{\mathrm{iso}}^{\mathrm{cut-off}})$ (erg)	γ	No. of Outliers	Simulated Sample: $\log_{10}$(True $E_{\mathrm{iso}}^{\mathrm{max}}$) (erg)	Simulated Sample: $\log_{10}$(Lower Limit on $E_{\mathrm{iso}}^{\mathrm{max}}$) (erg)	Catalog 2: $\log_{10}$(Lower Limit on $E_{\mathrm{iso}}^{\mathrm{max}}$) (erg)
1.93	**0.41**	**41.38**	**−1.30**	**9**	**42.15**	**42.09**	**42.16**
1.34	0.08	40.40	−2.04	61	40.96	40.96	41.89
1.34	0.08	40.40	0.99	199	41.42	41.41	41.66
1.34	0.08	42.46	−2.04	0	42.71	42.58	42.20
1.34	0.08	42.46	0.99	7	43.46	43.44	42.10
1.34	0.82	40.40	−2.04	291	40.87	40.86	41.58
1.34	0.82	40.40	0.99	434	41.44	41.43	41.47
1.34	0.82	42.46	−2.04	0	42.69	42.59	42.20
1.34	0.82	42.46	0.99	10	43.52	43.52	42.07
2.40	0.08	40.40	−2.04	510	40.83	40.83	41.42
2.40	0.08	40.40	0.99	1116	41.42	41.42	41.08
2.40	0.08	42.46	−2.04	0	42.99	42.78	42.20
2.40	0.08	42.46	0.99	30	43.47	43.46	41.97
2.40	0.82	40.40	−2.04	1042	40.85	40.84	41.11
2.40	0.82	40.40	0.99	1163	41.43	41.43	41.05
2.40	0.82	42.46	−2.04	0	43.09	42.85	42.20
2.40	0.82	42.46	0.99	51	43.54	43.54	41.91

Note. Same as Table 1.

ORCID iDs

Vishwangi Shah https://orcid.org/0000-0002-4823-1946
Jason W. T. Hessels https://orcid.org/0000-0003-2317-1446
Victoria M. Kaspi https://orcid.org/0000-0001-9345-0307
Kiyoshi W. Masui https://orcid.org/0000-0002-4279-6946
Mawson W. Sammons https://orcid.org/0000-0002-4623-5329
Daniel Amouyal https://orcid.org/0009-0005-5370-7653
Charanjot Brar https://orcid.org/0000-0002-1800-8233
Shami Chatterjee https://orcid.org/0000-0002-2878-1502
Alice P. Curtin https://orcid.org/0000-0002-8376-1563
Hannah Didehbani https://orcid.org/0009-0002-1640-1776
B. M. Gaensler https://orcid.org/0000-0002-3382-9558
Naman Jain https://orcid.org/0009-0009-0938-1595
Ronniy C. Joseph https://orcid.org/0000-0003-3457-4670
Afrokk Khan https://orcid.org/0009-0004-4176-0062
Bikash Kharel https://orcid.org/0009-0008-6166-1095
Adam E. Lanman https://orcid.org/0000-0003-2116-3573
Kyle McGregor https://orcid.org/0000-0003-2111-3437
Ryan Mckinven https://orcid.org/0000-0001-7348-6900
Mason Ng https://orcid.org/0000-0002-0940-6563
Kenzie Nimmo https://orcid.org/0000-0003-0510-0740
Ayush Pandhi https://orcid.org/0000-0002-8897-1973
Aaron B. Pearlman https://orcid.org/0000-0002-8912-0732
Alexander W. Pollak https://orcid.org/0000-0002-3430-7671
Paul Scholz https://orcid.org/0000-0002-7374-7119
Kaitlyn Shin https://orcid.org/0000-0002-6823-2073
Seth R. Siegel https://orcid.org/0000-0003-2631-6217
Kendrick Smith https://orcid.org/0000-0002-2088-3125
Michele Woodland https://orcid.org/0009-0001-3334-9482

References

Andersen, B. C., Patel, C., Brar, C., et al. 2023, AJ, 166, 138
Arcus, W. R., James, C., Ekers, R., et al. 2025, PASA, 42, e003
Bhandari, S., Heintz, K. E., Aggarwal, K., et al. 2022, AJ, 163, 69
Bhardwaj, M., Michilli, D., Kirichenko, A. Y., et al. 2024, ApJL, 971, L51
Bochenek, C. D., Ravi, V., Belov, K. V., et al. 2020, Natur, 587, 59
Caleb, M., Flynn, C., Bailes, M., et al. 2017, MNRAS, 468, 3746
CHIME Collaboration 2022, ApJS, 261, 29
CHIME/FRB Collaboration 2018, ApJ, 863, 48
CHIME/FRB Collaboration, Abbott, T. C., Amouyal, D., et al. 2025c, ApJL, 989, L48
CHIME/FRB Collaboration, Abbott, T., Andersen, B. C., et al. 2026, ApJS, 283, 34
CHIME/FRB Collaboration, Amiri, M., Andersen, B. C., et al. 2021, ApJS, 257, 59
CHIME/FRB Collaboration, Amiri, M., Andersen, B. C., et al. 2025b, ApJ, 993, 55
CHIME/FRB Collaboration, Amiri, M., Andersen, B. C., et al. 2024, ApJ, 969, 145
CHIME/FRB Collaboration, Amiri, M., Amouyal, D., et al. 2025a, ApJS, 280, 6
CHIME/FRB Collaboration, Andersen, B. C., Bandura, K., et al. 2023, ApJ, 947, 83
Cook, A. M., Bhardwaj, M., Gaensler, B. M., et al. 2023, ApJ, 946, 58
Cordes, J. M., & Lazio, T. J. W. 2002, arXiv:astro-ph/0207156
Cordes, J. M., Ocker, S. K., & Chatterjee, S. 2022, ApJ, 931, 88
Curtin, A. P., Sand, K. R., Pleunis, Z., et al. 2025, ApJ, 992, 206
Eftekhari, T., Dong, Y., Fong, W., et al. 2025, ApJL, 979, L22
Fonseca, E., Pleunis, Z., Breitman, D., et al. 2024, ApJS, 271, 49
Gordon, A. C., Fong, W.-f., Kilpatrick, C. D., et al. 2023, ApJ, 954, 80
Heintz, K. E., Prochaska, J. X., Simha, S., et al. 2020, ApJ, 903, 152
Hu, C.-P., Wadiasingh, Z., Ho, W. C. G., et al. 2025, ApJ, 989, 63
Hurley, K., Boggs, S. E., Smith, D. M., et al. 2005, Natur, 434, 1098
James, C. W., Prochaska, J. X., Macquart, J. P., et al. 2022, MNRAS, 509, 4775
Kaspi, V. M., & Beloborodov, A. M. 2017, ARA&A, 55, 261
Kirsten, F., Marcote, B., Nimmo, K., et al. 2022, Natur, 602, 585
Kirsten, F., Ould-Boukattine, O. S., Herrmann, W., et al. 2024, NatAs, 8, 337
Kumar, P., Lu, W., & Bhattacharya, M. 2017, MNRAS, 468, 2726
Lanman, A. E., Andrew, S., Lazda, M., et al. 2024, AJ, 168, 87
Li, D., & Pen, U.-L. 2024, MNRAS, 531, 2330
Lorimer, D. R., Bailes, M., McLaughlin, M. A., Narkevic, D. J., & Crawford, F. 2007, Sci, 318, 777
Luo, R., Men, Y., Lee, K., et al. 2020a, MNRAS, 494, 665
Luo, R., Wang, B. J., Men, Y. P., et al. 2020b, Natur, 586, 693
Lyubarsky, Y. 2014, MNRAS, 442, L9
Lyutikov, M. 2021, ApJ, 922, 166
Lyutikov, M., & Popov, S. 2020, arXiv:2005.05093
Macquart, J. P., Prochaska, J. X., McQuinn, M., et al. 2020, Natur, 581, 391
Mckinven, R., Bhardwaj, M., Eftekhari, T., et al. 2025, Natur, 637, 43
McQuinn, M. 2014, ApJL, 780, L33
Metzger, B. D., Margalit, B., & Sironi, L. 2019, MNRAS, 485, 4091
Nimmo, K., Hessels, J. W. T., Kirsten, F., et al. 2022, NatAs, 6, 393
Ofek, E. O., Kulkarni, S. R., Nakar, E., et al. 2006, ApJ, 652, 507
Ould-Boukattine, O. S., Chawla, P., Hessels, J. W. T., et al. 2026, MNRAS, 545, staf1937
Petroff, E., Hessels, J. W. T., & Lorimer, D. R. 2022, A&ARv, 30, 2
Planck Collaboration, Aghanim, N., Akrami, Y., et al. 2020, A&A, 641, A6
Pleunis, Z., Good, D. C., Kaspi, V. M., et al. 2021, ApJ, 923, 1
Prochaska, J. X., & Zheng, Y. 2019, MNRAS, 485, 648
Ravi, V., Catha, M., D'Addario, L., et al. 2019, Natur, 572, 352
Ryder, S. D., Bannister, K. W., Bhandari, S., et al. 2023, Sci, 382, 294
Schnitzeler, D. H. F. M. 2012, MNRAS, 427, 664
Shah, V., Shin, K., Leung, C., et al. 2025, ApJL, 979, L21
Shannon, R. M., Macquart, J.-P., Bannister, K. W., et al. 2018, Natur, 562, 386
Sharma, K., Ravi, V., Connor, L., et al. 2024, Natur, 635, 61
Shin, K., Masui, K. W., Bhardwaj, M., et al. 2023, ApJ, 944, 105
Snelders, M. P., Nimmo, K., Hessels, J. W. T., et al. 2023, NatAs, 7, 1486
Sun, W.-P., Cao, Y.-L., Zhang, Y.-K., et al. 2026, SCPMA, 69, 109512
Yamasaki, S., & Totani, T. 2020, ApJ, 888, 105
Younes, G., Güver, T., Kouveliotou, C., et al. 2020, ApJL, 904, L21
Zhang, J.-S., Wang, T.-C., Wang, P., et al. 2025, arXiv:2507.14707